Biosurface and Biotribology

WILEY

The Institution of Engineering and Technology

ORIGINAL RESEARCH OPEN ACCESS

Effects of Braiding Parameters on the Mechanical and Tribological Properties of Artificial Ligaments

Jian Song[1] | Guiyang Liu[1,2] | Shenglin Li[1] | Xuanye Liu[3] | Yeping Peng[2]

[1]School of Biomedical Engineering, Sun Yat-sen University, Guangzhou, China | [2]Guangdong Key Laboratory of Electromagnetic Control and Intelligent Robots, College of Mechatronics and Control Engineering, Shenzhen University, Shenzhen, China | [3]Shady Side Academy, Pittsburgh, Pennsylvania, USA

Correspondence: Yeping Peng (yeping.peng@szu.edu.cn)

Received: 27 May 2025 | **Revised:** 15 February 2026 | **Accepted:** 21 March 2026

Keywords: anterior cruciate ligament reconstruction | artificial ligament | braiding parameters | mechanical and tribological properties

ABSTRACT

Artificial ligaments (ALs), as important grafts for reconstructing the anterior cruciate ligament, often fail in rupture owing to inadequate mechanical properties and frictional wear in clinical practice. Braiding parameters affect the properties of ALs. Previous studies have been limited to investigating the effects of braiding parameters on the mechanical or tribological properties of ALs in isolation and lacked a comprehensive investigation into their combined or synergistic impact. Therefore, in this study, ALs with different braiding parameters are prepared, and mechanical and tribological indicators are integrated to conduct a synergistic investigation. The results show that as the braiding angle and number of layers decrease, the breaking strain increases, while the ultimate tensile force, elastic modulus, and yield force decrease. The number of spindles positively correlates with the mechanical and tribological performance of ALs.

1 | Introduction

The knee is one of the largest and most complex joints in the human body. The anterior cruciate ligament serves as an important component in maintaining joint stability and normal motor function [1]. It connects the femur and tibia, effectively preventing the tibia from excessive anterior displacement and the knee joint from excessive rotation. However, the anterior cruciate ligament (ACL) is susceptible to fracture or injury during strenuous exercise or trauma, resulting in knee joint instability and functional limitations [2]. Moreover, the ACL has limited self-repairing ability. It does not readily heal on its own once fracture occurs, such that injury usually requires surgical reconstruction [3]. In ACL reconstruction surgery, artificial ligaments are considered a better choice than autografts and allografts as they do not introduce risks of donor site injury and disease transmission [4, 5].

Ideal artificial ligaments (ALs) require excellent mechanical properties to withstand complex loads of the knee joint during daily activities and strenuous sports and to maintain joint stability and motor function [6]. Inadequate mechanical properties may lead to laxity, rupture, or failure of the ligament [7]. In addition, excellent frictional properties are required to reduce wear and tear on the surface of the AL during movement, prolonging the life of the material while reducing the risk of inflammation or tissue damage caused by friction with surrounding tissues [8, 9]. The mechanical and tribological properties of ALs affect the treatment and rehabilitation of injured patients, and the braiding parameters directly determine the mechanical and tribological properties of ALs. It is thus important to explore the effects of braiding parameters on the mechanical and tribological properties of ALs.

The effects of braiding parameters on the mechanical and tribological properties of Als have been extensively investigated through tensile fracture tests [10, 11], cyclic loading tensile tests [12, 13], and in vitro friction and wear experiments [14]. Although these studies explored the effects of braiding parameters on the mechanical and tribological properties of ALs, they

TABLE 1 | Braiding scheme for AL experimental samples with different braiding parameters.

Braiding schemes	AL1-1	AL1-2	AL2-1	AL2-2	AL3-1	AL3-2
A (°)	45.00	30.00	45.00	45.00	45.00	45.00
S	24.00	24.00	24.00	18.00	24.00	24.00
LY	1.00	1.00	2.00	2.00	2.00	1.00

often focused on either the mechanical or tribological properties rather than the synergistic effect of the two types of property, making it difficult to truly reflect the overall performance of ALs in the complex physiological environment of the knee joint. This study investigates the properties of ALs by integrating mechanical and tribological indicators and analyzes the effects of different braiding parameters on the mechanical and tribological properties of ALs, so as to provide more comprehensive guidance for the design and optimisation of ALs.

The remainder of the paper is structured as follows. Section 2 outlines the experimental procedures for the preparation of ALs, along with the methods used for testing their mechanical and tribological properties, and capturing their micro-morphological features. Section 3 discusses the effects of different braiding parameters on the mechanical and tribological properties of ALs. Conclusions are drawn from the results of the study in Section 4.

2 | Methods and Experiments

This study explores the effects of braiding parameters on the properties of ALs. First, AL experimental samples with different braiding parameters are prepared by changing a single braiding parameter. Then, in terms of mechanical properties, the experimental samples are subjected to mechanical tensile testing to obtain mechanical properties such as the breaking strain (BS), ultimate tensile force (UTF), elastic modulus (EM), and yield force (YF), and the effects of different braiding parameters on the mechanical properties of ALs are analyzed. Finally, in terms of tribological properties, the tribological properties of ALs with different braiding parameters are analyzed by combining wear information, such as the wear surface morphology, coefficient of friction, and wear debris size and morphological distributions.

2.1 | Sample Preparation

Six groups of AL samples having different braiding parameters are prepared. The groups are labelled AL1-1, AL1-2, AL2-1, AL2-2, AL3-1, and AL3-2, corresponding to different braiding angles (*A*), number of spindles (*S*), and number of layers (LY). Polyethylene terephthalate (PET) yarn (150 denier) is used as the material for AL experimental samples, owing to its excellent mechanical properties and biocompatibility. A braiding machine (XH 90-24, Xianghai Braider, China) is used to prepare the AL experimental samples. The parameter settings are as follows. The braiding angles of the AL1 series are set at 45° and 30°, the number of spindles of the AL2 series are set at 24 and 18, and the number of layers of the AL3 series are set at two and one layers. At least three parallel samples are prepared for each type of AL to ensure statistical reliability of performance tests. Polyetheretherketone (PEEK) balls are widely used in medical applications such as artificial joints and dental implants for their excellent mechanical properties, good biocompatibility, and a modulus of elasticity similar to that of natural bone [15]. A PEEK ball with a diameter of 5 mm is used as the upper friction pair in the friction experiments, whereas AL samples with varying braiding parameters serve as the lower friction counterparts, as shown in Table 1.

2.2 | Mechanical Tests of ALs

The mechanical properties of the braided ALs are evaluated using a universal testing machine (Instron 5969, Illinois Tool Works Inc., USA) with a 50-kN force sensor. The scale distance is set at 100 mm and the sample testing speed at 100 mm/min. Before conducting the mechanical tensile experiments, a preload of 5 N is applied to the experimental samples to ensure that the samples are in a tensile state. The breaking strain, ultimate tensile force, elastic modulus, and yield force are selected as key parameters for characterising the mechanical performance.

2.3 | Tribological Tests on ALs

The friction experiment is carried out on ALs using a multifunctional friction testing machine manufactured by Rtec Company. As shown in Figure 1, the upper friction pair of the PEEK ball is fixed below the force sensor through a cylindrical fixture, while the experimental sample of the AL is fixed in a square stage by the lower friction pair fixture. The stage is designed to hold lubricating media, such as phosphate buffered saline. The normal load applied by the testing machine is set at 5 N, the frequency is 2 Hz, the running time is 20 min, and the stroke is 3 mm. Three replicates of each experimental sample are used to eliminate the effect of accidental errors on the results. The friction testing machine is used to achieve linear reciprocating motion and record the curve of the coefficient of friction in real time.

2.4 | Microscopy

The two-dimensional (2D) wear surface morphology and wear debris characteristics of the AL experimental samples are observed under a Quanta 250 FEG scanning electron microscope (SEM) manufactured by FEI, USA. After the friction experiment, the AL experimental samples are removed, and the wear liquid is collected in a centrifuge tube for the observation

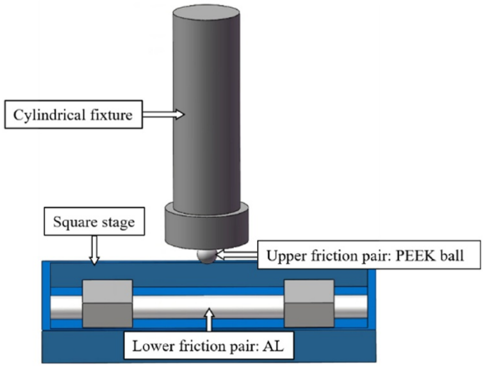

FIGURE 1 | Schematic of the friction pair clamping module.

of wear debris. The ALs are dried at 37°C for 24 h and placed on a stage with conductive tape for 120 s of gold spraying to enhance the conductivity of the sample surface. This is followed by SEM observation. The size and morphological of the wear debris are statistically analyzed using ImageJ software. The wear debris is mainly classified into elongated, flaky, blocky, and near-circular categories, as shown in Figure 2.

In addition, the three-dimensional (3D) wear surface morphology of the experimental samples of the ALs is observed using a VK-250 laser scanning confocal microscope (LSCM) manufactured by KEYENCE, Japan. Moreover, multi-file analysis software supplied with the LSCM is used to calculate the statistical parameters of the surface morphology of the AL wear area, including the surface arithmetic mean height, surface root mean square height, and surface maximum height, for quantification of the 3D micro-morphological characteristics of the wear area of the AL from multiple directions. The definitions and corresponding equations of the relevant parameters are provided below.

The surface arithmetic mean height (*Sa*) represents the arithmetic mean of the absolute coordinates z (x, y) in a specified area (i.e., the mean absolute height) and is used to describe the overall height deviation of the surface. It is expressed as

$$Sa = \frac{1}{A}\iint_A |z(x, y)| dxdy, \tag{1}$$

where A is the area of the specified area, x is the abscissa of the specified point, y is the ordinate of the specified point, and z (x, y) is the height value of the specified point.

The surface root mean square height (*Sq*) is the root mean square of the height of each point in the specified area, which is equivalent to the standard deviation of the height. It is expressed as

$$Sq = \sqrt{\frac{1}{A}\iint_A z^2(x, y) dxdy}. \tag{2}$$

The surface maximum height (*Sz*) is the sum of the maximum peak height and the maximum valley depth in the area. It is expressed as

$$Sz = Sp + |Sv|, \tag{3}$$

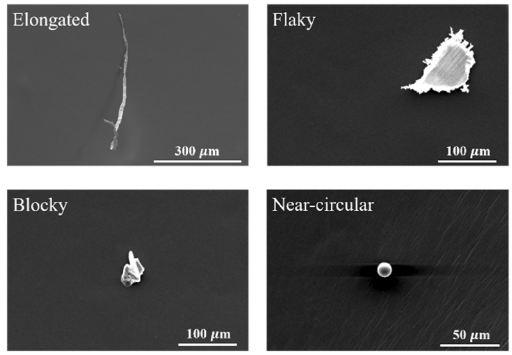

FIGURE 2 | Partial SEM images of different wear debris morphologies of AL.

where *Sp* is the height of the highest point in the area and *Sv* is the height of the lowest point in the area.

3 | Results and Discussion

3.1 | Effects of the Braiding Angle on the Properties of ALs

AL experimental samples, labelled AL1-1 and AL1-2, are processed with angles of 45° and 30° to explore the effects of the braiding angle on the properties of ALs. The braiding angle of these samples directly affects the arrangement of the fibres in the structure, enabling the systematic evaluation of the effects of the braiding angle on the mechanical and tribological properties of the ALs [16]. Data on the mechanical properties, such as the breaking strain, ultimate tensile force, elastic modulus, and yield force, are obtained to evaluate the mechanical performance of the ALs. The results are given in Table 2.

Table 2 reveals that, as the braiding angle decreases, the BS of the AL increases by 9.91%, while the UTF, EM, and YF decrease by 0.31%, 5.23%, and 0.73%, respectively. Specifically, a smaller braiding angle means that the fibres in the braided structure are oriented more transversely, and the degree of interlacing between the fibres increases [3]. The fibres undergo increased slipping and deformation before reaching breaking point, resulting in a higher BS and enhanced ductility and flexibility. However, this structure reduces the fibre component force in the tensile direction, making it difficult for the fibres to bear loads directly and reducing the UTF, EM, and YF.

It has been shown that during friction experiments on ALs, some silk threads of the ALs break through fatigue damage at the microstructural level. The fibre structure shows a drawn and loose state and is accompanied by material shedding [17]. At the same time, pits form on the wear surface of the samples, which increases surface roughness and reduces the tribological properties of the material [18]. Therefore, the tribological properties of ALs are evaluated by observing the morphological changes of the worn surface and the statistical parameters of the surface morphology. A smoother worn surface corresponds to fewer fibre draws, less material spalling, and better tribological properties of the ALs. According to the above surface morphology statistical parameters, the morphology characteristic parameters

TABLE 2 | Mechanical properties of ALs with different braiding angles.

Braiding schemes	*A* (°)	*S*	LY	BS (100%)	UTF (N)	EM (MPa)	YF (N)
AL1-1	45.00	24.00	1.00	2.12	4454.31	58.73	3074.27
AL1-2	30.00	24.00	1.00	2.33	4440.63	55.66	3051.68

of the original and worn samples of the ALs are calculated and shown in Table 3.

Figure 3 presents 2D SEM images and 3D LSCM images of wear surfaces of the AL experimental samples with different braiding angles. These images visually illustrate the microstructural surface changes and wear characteristics, which can be further analyzed in conjunction with the data in Table 3. Among the AL experimental samples with different braiding angles, AL1-1 has the smallest wear area, mainly located on its outer shell. Its fibre surface is smoother than the surfaces of the other AL samples, having fewer fibre draws and less material spalling. In addition, AL1-1 has the lowest surface morphology parameters—*Sa*, *Sq*, and *Sz*—measured as 157.98, 205.01, and 1370.96 μm, respectively. These results indicate the smallest height deviation of the wear surface during friction and a shallow overall depth of abrasion, and a relatively smooth and uniform surface texture, suggesting superior tribological performance. In contrast, AL1-2 has the largest wear area, with extensive fibre pull-out and material spalling, indicating more severe wear during friction. Its surface morphology parameters—*Sa*, *Sq*, and *Sz*—are higher at 229.09, 277.53 and 1819.30 μm with an increase of 45.01%, 35.37% and 32.70%, respectively. This reflects a rougher, more irregular wear surface and poorer tribological performance compared with AL1-1.

To reduce the risk of bone tunnel enlargement after AL implantation in the human body, Li et al. pointed out that shell-layer structured ALs with different fibre ratios can be prepared by adding smoother PET monofilament materials, effectively enhancing the tribological properties of ALs. A smaller coefficient of friction (COF) corresponds to better tribological properties of ALs [19]. The COF is thus adopted to evaluate the tribological performance of ALs.

All experimental samples in this study are tested under the same working conditions. Considering that the wear of ALs presents a progressive characteristic of fibre abrasion and breakage sequentially, the wear in long and short testing periods only corresponds to the abrasion process of different fibres, and the properties of each fibre strand are assumed to be consistent in this study. Based on reports in existing literature [19], the duration of the friction test is set to 20 min to ensure that the differences in experimental results arise only from the different braiding parameters of the ALs. After the experiments are completed, the original data exported from the friction experimental machine are smoothed to eliminate noise interference and improve the accuracy of the data. Subsequently, the data are summarised and organised. COF–time curves of the experimental samples of ALs with different braiding angles are plotted in Figure 4. These curves show the trend of the COF with time during the friction experiments of ALs with different braiding angles and clearly reflect differences among the groups.

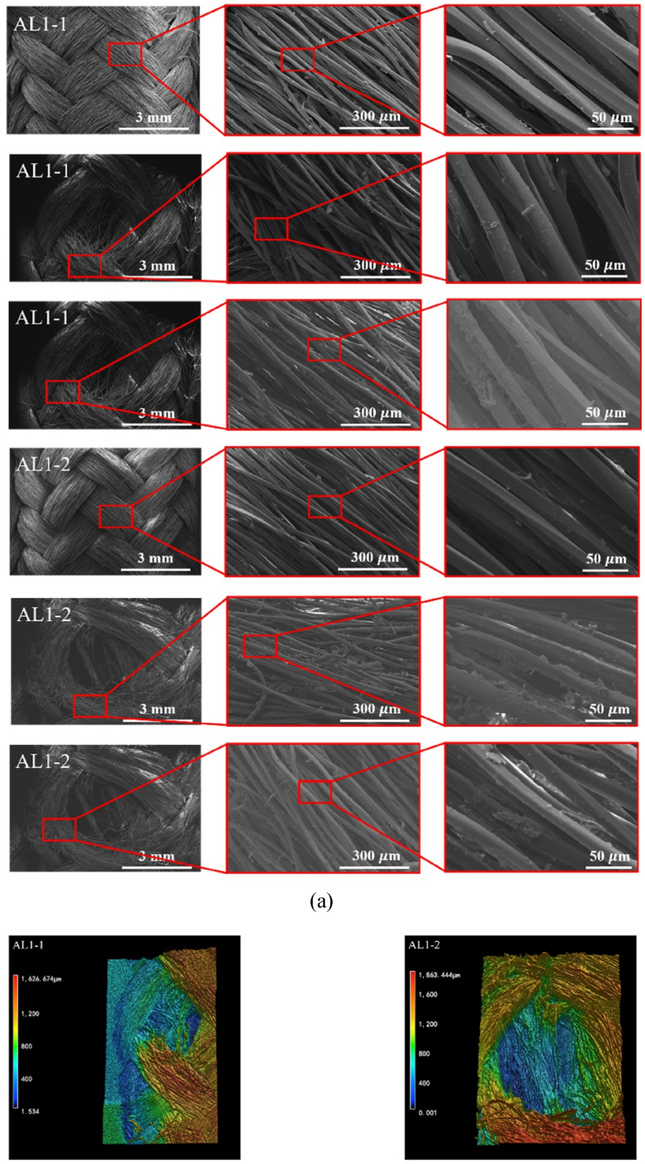

(b)

FIGURE 3 | Wear surface morphologies of ALs having different braiding angles: (a) 2D SEM images of original and worn samples, (b) 3D LSCM images of worn samples.

TABLE 3 | Surface morphology characteristic parameters of original and worn ALs with different braiding angles.

Braiding schemes	States	*Sa* (μm)	*Sq* (μm)	*Sz* (μm)
AL1-1	Original	62.11	75.5	465.65
	Worn	157.98	205.01	1370.96
AL1-2	Original	67.93	83.64	498.46
	Worn	229.09	277.53	1819.30

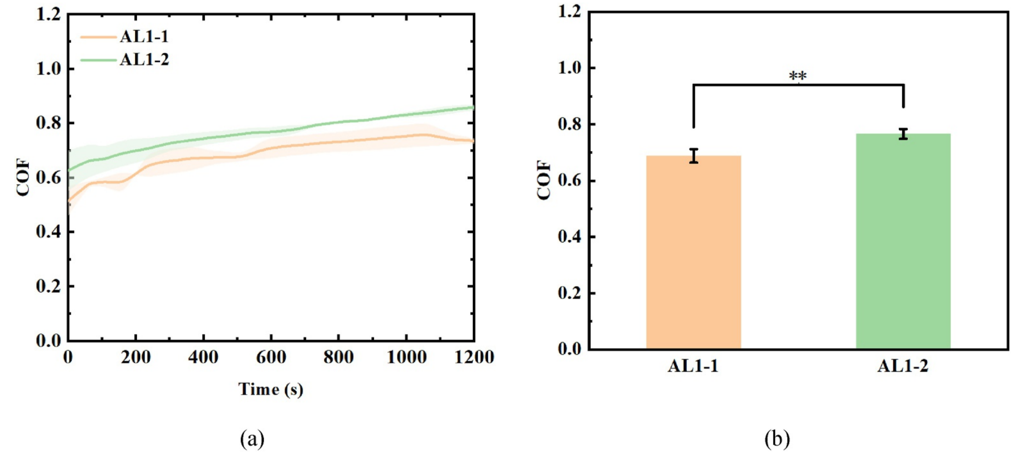

FIGURE 4 | ALs with different braiding angles: (a) COF–time trend, (b) COF significance analysis. The data are the mean ± SD ($n = 3$; p values are calculated using one-way ANOVA with Tukey correction, *$p < 0.05$, **$p < 0.01$, ***$p < 0.001$).

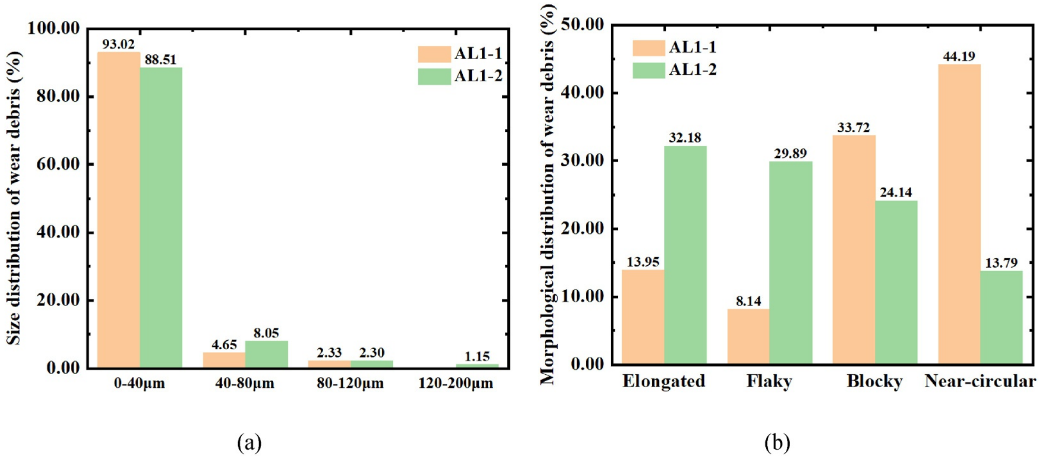

FIGURE 5 | Wear debris of ALs with different braiding angles: (a) Size distribution, (b) morphological distribution.

Figure 4 shows that among the AL experimental samples with different braiding angles, AL1-1 consistently has the lowest COF, indicating minimal frictional resistance throughout the testing process and superior tribological performance. In contrast, AL1-2 consistently has the highest COF, reflecting greater frictional resistance, more severe surface wear, and inferior tribological properties.

The size and morphological distribution of wear debris from AL samples with different braiding angles are statistically analyzed using ImageJ, as shown in Figure 5. AL1-1 has the highest proportion of small-sized wear debris (0–40 μm), accounting for 93.02%, and the lowest percentage of medium-sized wear debris (40–120 μm) at only 6.98%. No large-sized wear debris (larger than 120 μm) is observed. In addition, AL1-1 has the largest proportion of near-circular wear debris, reaching 44.19%. This distribution pattern indicates that AL1-1 undergoes the least wear, with the debris mainly comprising fine particles generated by slight surface fibre abrasion. The wear surface of AL1-1 exhibits relatively smooth morphological characteristics, reflecting its excellent tribological properties during friction. In contrast, AL1-2 has a reduced proportion of small-sized debris and larger proportions of medium-sized and large-sized debris. The percentage of medium-sized wear debris (40–120 μm) is 10.35%, and the percentage of large-sized debris (greater than 120 μm) is 1.15%. Regarding debris shape, the percentage of near-circular debris of AL1-2 decreases to 13.79%, whereas elongated debris has the highest percentage at 32.18%. AL1-2 thus undergoes the most severe wear, with pronounced changes in surface morphology characterised by fibre breakage and material spalling, highlighting its comparatively poor tribological properties.

Overall, the tribological properties of ALs deteriorate as the braiding angle decreases. Specifically, the reduced braiding angle makes the arrangement of fibres in the structure more transverse. This increases the interlacing of the fibres and exposes more surface area, leading to an increase in surface roughness [20]. The increased contact area and number of points between fibres and the friction surfaces increase the COF. In addition, a smaller braiding angle makes it easier for slippage and relative movement between the fibres to occur. During friction, this is likely to generate more wear debris and surface damage, further exacerbating the wear. Meanwhile, the braided structure loosens, and the supporting force between the fibres weakens, reducing the material's resistance to friction and making it more prone to deformation and material loss during dynamic sliding.

3.2 | Effects of the Number of Spindles on the Properties of ALs

To explore the effects of the number of spindles on the properties of ALs, two braiding processes using 24 and 18 spindles are employed to prepare AL experimental samples, respectively labelled AL2-1 and AL2-2. The variation in the spindle count for these samples directly affects the braiding density and structural tightness of the fibres and thus the mechanical and tribological properties [21]. Similarly, mechanical tensile tests are carried out to evaluate the mechanical performance. The results are given in Table 4.

Table 4 shows that a decrease in the number of spindles reduces the BS, UTF, EM, and YF of the ALs by 41.04%, 24.80%, 25.00%, and 32.93%, respectively. Specifically, fewer spindles lead to a lower braiding density, less interweaving between fibres, and a looser structure [22]. The component force of the fibre in the tensile direction weakens, impairing effective load transfer and thus reducing the UTF, EM, and YF. In addition, the looser structure increases the sliding space between fibres, making the material more prone to deformation during the tensile process and reducing the BS. Moreover, the uneven distribution of fibres becomes more pronounced, leading to localised stress concentrations that further compromise the overall mechanical properties of the AL.

According to the statistical parameters of surface topography, the morphological characteristics of the original and worn AL experimental samples with different spindle counts are calculated, as shown in Table 5. A decrease in the number of spindles increases all the morphological characteristics of the wear areas by 11.4%, 7.02% and 22.07%, respectively. The 2D and 3D wear surface morphological images of the AL experimental samples with different spindle counts are shown in Figure 6. By analyzing Table 5 alongside the surface morphology images, it is found that AL2-1 has a smaller wear area, a relatively smooth surface morphology, and the shallowest wear depth, indicating minimal surface damage and superior tribological performance. In contrast, AL2-2 shows the largest wear area, with pronounced fibre pull-out and material spalling. The wear depth is greatest, and the surface morphology changes are more severe, reflecting a higher degree of wear and inferior tribological properties.

The COF–time curves for AL samples with different spindle counts are plotted in Figure 7. Consistent with previous analyses, AL2-1 has the best tribological performance, characterised by the lowest COF, and minimal frictional resistance. In

TABLE 5 | Surface morphology characteristic parameters of original and worn ALs with different spindle counts.

Braiding schemes	States	*Sa* (μm)	*Sq* (μm)	*Sz* (μm)
AL2-1	Original	92.53	112.74	748.27
	Worn	269.11	322.80	1714.42
AL2-2	Original	113.99	140.35	790.70
	Worn	299.80	345.46	2092.75

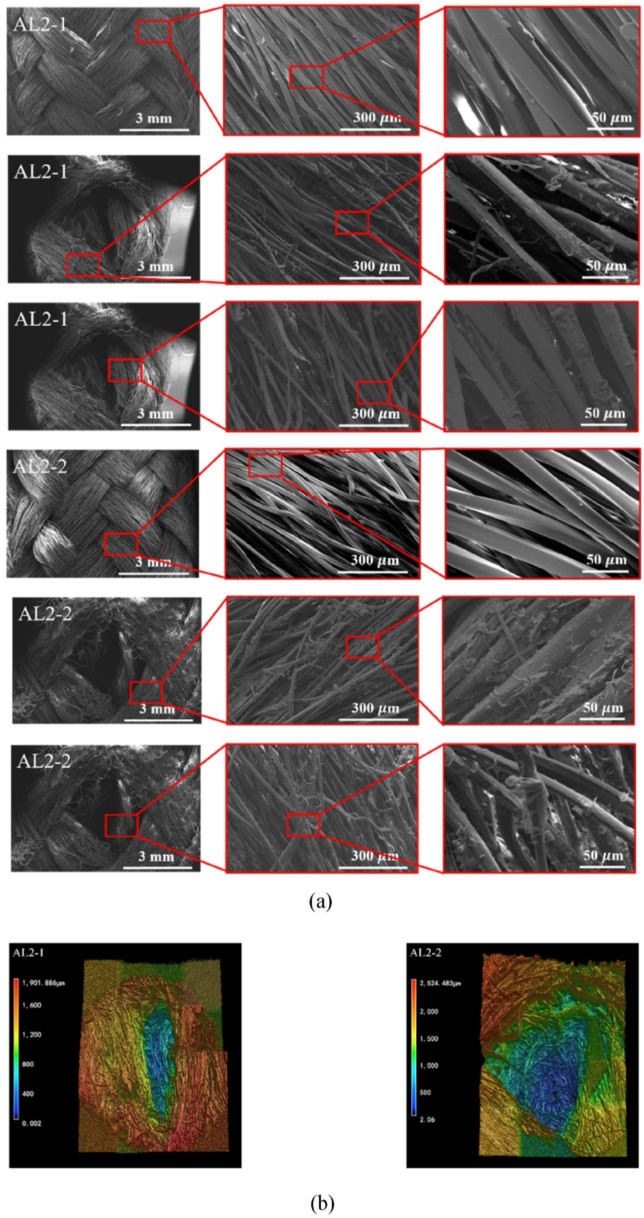

FIGURE 6 | Wear surface morphologies of ALs with different spindle counts: (a) 2D SEM images of original and worn samples, (b) 3D LSCM images of worn samples.

TABLE 4 | Mechanical properties of ALs with different spindle counts.

Braiding schemes	A (°)	S	LY	BS (100%)	UTF (N)	EM (MPa)	YF (N)
AL2-1	45.00	24.00	2.00	2.12	4176.02	54.01	3092.31
AL2-2	45.00	18.00	2.00	1.25	3140.26	40.51	2073.98

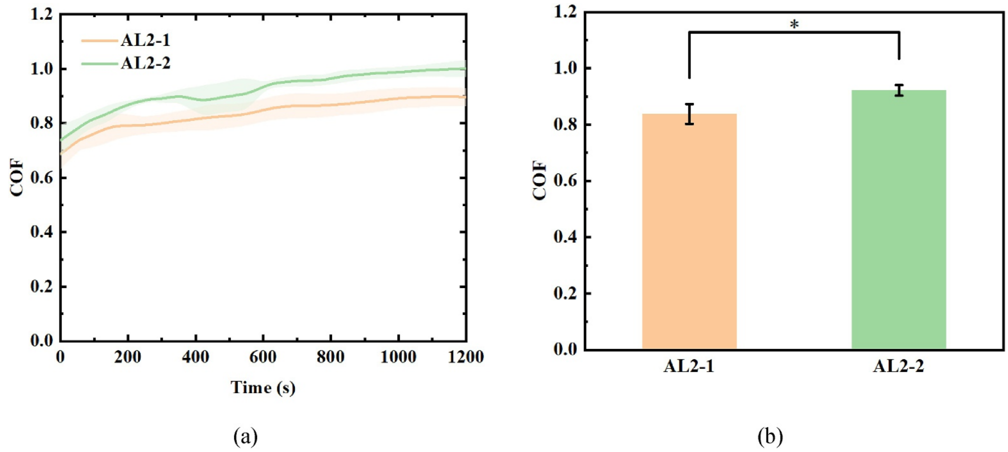

FIGURE 7 | ALs with different spindle counts: (a) COF–time trend, (b) COF significance analysis. The data are the mean ± SD ($n = 3$; p values are calculated using one-way ANOVA with Tukey correction, *$p < 0.05$, **$p < 0.01$, ***$p < 0.001$).

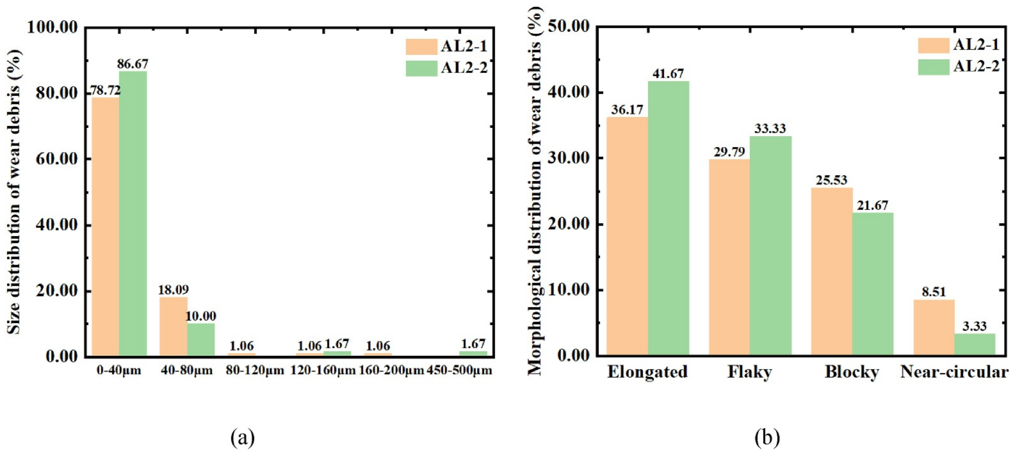

FIGURE 8 | Wear debris of ALs with different spindle counts: (a) Size distribution, (b) morphological distribution.

contrast, AL2-2 has higher COF values, indicating greater frictional resistance and poorer tribological properties.

Figure 8 presents the size and morphological distributions of wear debris for ALs with different spindle counts. Using the same analytical approach as before, insights are gained from the wear debris characteristics. AL2-1 exhibits the least wear, with debris predominantly in the small-size range, indicating superior tribological performance. In contrast, AL2-2 shows the most significant wear, including the presence of large-sized debris ranging from 450 to 500 μm, reflecting its comparatively poor tribological properties.

Overall, the tribological properties of ALs deteriorate as the number of spindles decreases. Specifically, a decrease in the number of spindles causes a reduction in braiding density, less interweaving among fibres, a looser structure, lower surface flatness, and increased fibre exposure, all of which result in higher surface roughness [23]. During friction, there are more contact points on the rough surface, and the COF increases. At the same time, the loose structure makes the fibres more prone to slip and spalling, generating more wear debris and aggravating the wear. In addition, the reduction in the number of spindles decreases the compactness of the structure and weakens the resistance of the material to frictional stresses, leading to reduced wear resistance. Therefore, the loosening of the structure and the increase in surface roughness caused by the reduction in the number of spindles are the main reasons for the deterioration of tribological properties.

3.3 | Effects of the Number of Layers on the Properties of ALs

To explore the effects of the number of layers on the properties of ALs, single-layer and double-layer braiding processes are adopted to prepare AL experimental samples, labelled as AL3-1 and AL3-2. The number of layers in these samples directly affects the stacking density and structural stability of the fibres and thus the mechanical and tribological properties [24]. The results of mechanical tensile tests are given in Table 6.

Table 6 shows that, as the number of layers decreases, the BS of the ALs increases by 2.58%, whereas the UTF, EM, and YF decrease by 6.65%, 12.57%, and 1.24%, respectively. Specifically, the decrease in the number of braiding layers reduces the stacking of fibres and thus loosens the structure [25]. The

TABLE 6 | Mechanical properties of ALs with different layer counts.

Braiding schemes	*A* (°)	*S*	LY	BS (100%)	UTF (N)	EM (MPa)	YF (N)
AL3-1	45.00	24.00	2.00	1.94	4081.40	46.61	3031.59
AL3-2	45.00	24.00	1.00	1.99	3809.87	40.75	2994.05

TABLE 7 | Surface morphology characteristic parameters of original and worn ALs with different layer counts.

Braiding schemes	States	*Sa* (μm)	*Sq* (μm)	*Sz* (μm)
AL3-1	Original	87.16	101.67	507.38
	Worn	257.86	305.44	1445.70
AL3-2	Original	64.78	77.11	481.54
	Worn	167.88	199.89	1189.75

mutual support and binding force between fibres decrease, allowing the material to experience more slippage and deformation during the tensile process and thus increasing the BS and enhancing ductility. However, the reduction in the number of layers reduces the load distribution capacity, effective load-bearing area of the fibres in the tensile direction, and thus the UTF, EM, and YF. In addition, the single-layer structures are more prone to localised stress concentrations, further weakening the overall rigidity and deformation resistance of the material, such that the mechanical performance indicators decrease.

According to the statistical parameters of surface topography, the morphological characteristic parameters of the original and worn AL experimental samples with different layer counts are calculated as shown in Table 7. As the number of layers decreases, all morphological characteristic parameters of the wear areas decrease by 53.60%, 52.80% and 21.51%, respectively. Figure 9 presents 2D and 3D wear surface morphological images of the AL experimental samples with different layer counts. By analyzing these data using the same methodology as before, it is found that AL3-1 has a larger wear area. In addition, AL3-1 has the greatest wear depth and the greatest changes in surface morphology, indicating severe wear and poor tribological performance. In contrast, AL3-2 has the smallest wear area, relatively flat surface morphology, shallower wear depth, and a slight change in the surface morphology—indicating a lower degree of wear and superior tribological properties.

COF–time curves for the AL experimental samples with layer counts are plotted in Figure 10. Consistent with previous analyses, AL3-1 has the highest COF, indicating greater frictional resistance and poorer tribological performance. In contrast, AL3-2 has the lowest COF, reflecting minimal frictional resistance and superior tribological properties.

Figure 11 presents the size and morphological distributions of wear debris for ALs with different layer counts. Using the same analytical approach as before, it is found that AL3-1 experiences the greatest wear, characterised by a higher proportion of medium- and large-sized debris, reflecting poorer tribological performance. In contrast, AL3-2 exhibits the least wear, with debris mainly comprising small-sized wear debris, indicating better tribological properties.

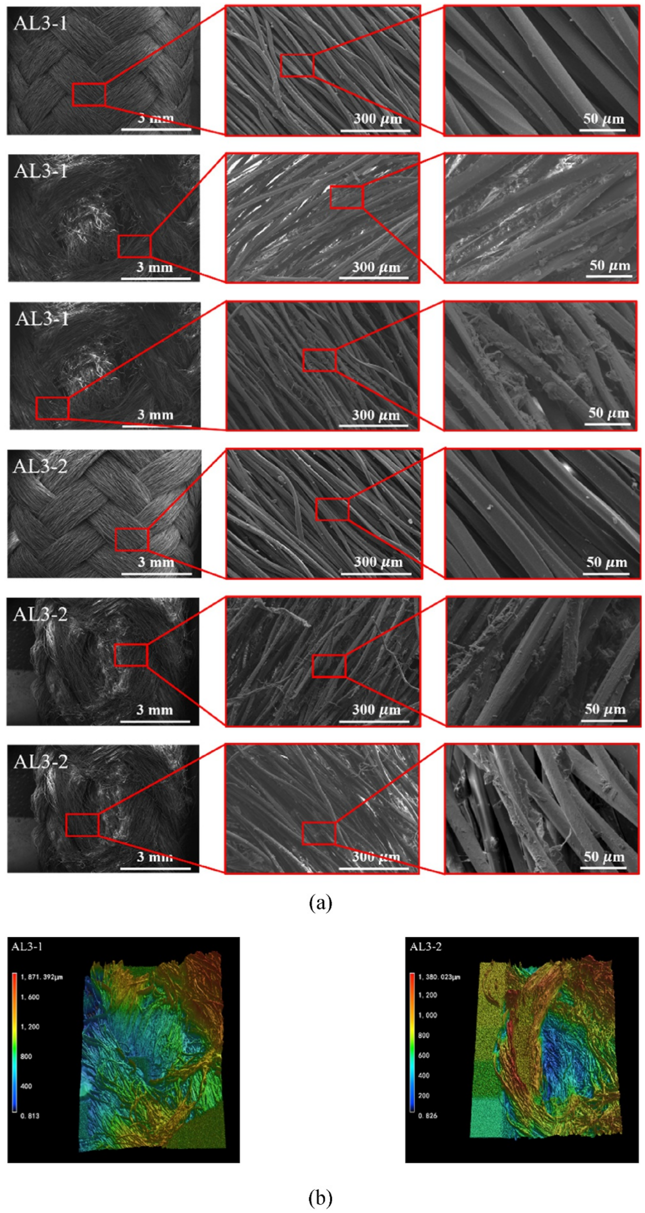

FIGURE 9 | Wear surface morphologies of ALs with different layer counts: (a) 2D SEM images of original and worn samples, (b) 3D LSCM images of worn samples.

Overall, the tribological properties of ALs improve as the number of layers decreases. Specifically, a reduction in the number of layers leads to a lower stacking density of fibres, making the structure looser and reducing the surface rigidity. With less interweaving between fibres, the surface roughness decreases, reducing the number of contact points with the friction surface, the frictional resistance, and thus the COF. In addition, fewer layers result in a more uniform stress distribution of fibres during friction, reducing the likelihood of local

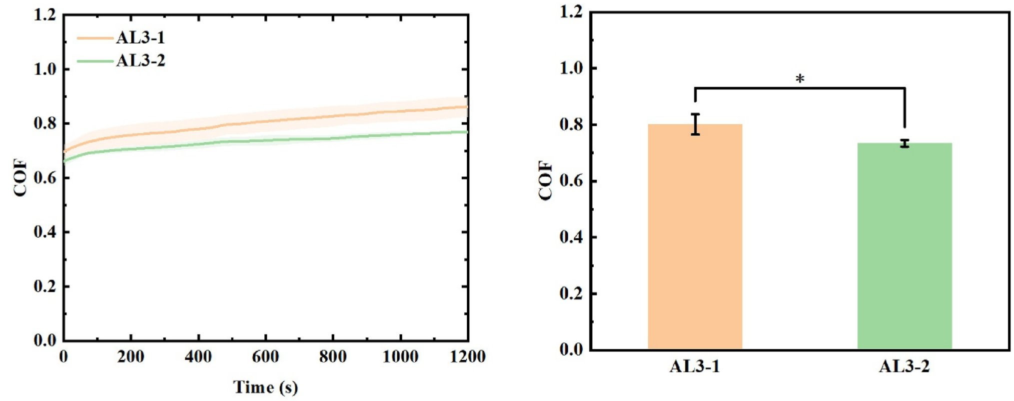

(a) (b)

FIGURE 10 | ALs with different layers counts: (a) COF–time trend, (b) COF significance analysis. The data are the mean ± SD ($n = 3$; p values are calculated using one-way ANOVA with Tukey correction, *$p < 0.05$, **$p < 0.01$, ***$p < 0.001$).

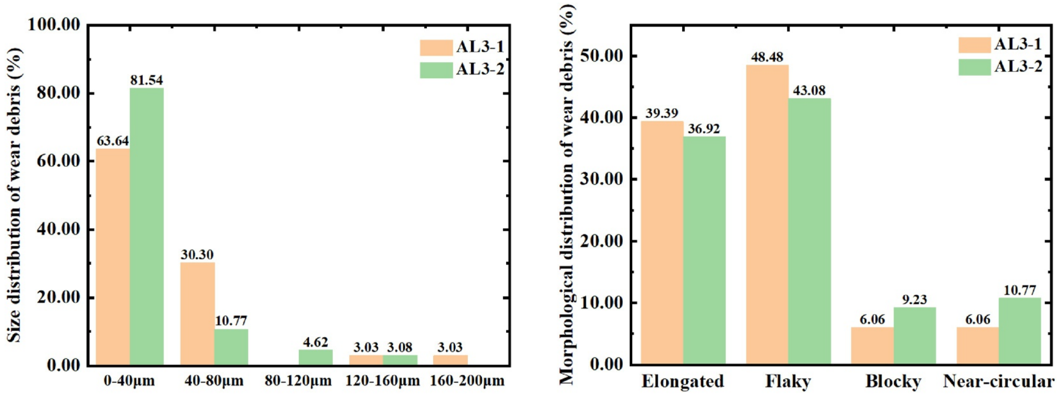

(a) (b)

FIGURE 11 | Wear debris of ALs with different layer counts: (a) Size distribution, (b) morphological distribution.

wear and material peeling and improving tribological properties. Furthermore, in clinical applications, the braiding parameters of ALs with superior tribological performance are selected based on patients' actual conditions, on the premise that the mechanical performance of ALs is prioritised to meet clinical requirements.

4 | Conclusions

The effects of braiding parameters on the mechanical and tribological properties of ALs were explored. The following conclusions are drawn from the experimental results.

1. Decreasing the braiding angle increases the breaking strain of the AL by 9.91%, and decreases mechanical properties such as the ultimate tensile force, elastic modulus and yield force by a maximum of 5.23%. Moreover, the tribological properties deteriorates by a maximum of 45.01%.
2. Reducing the number of spindles negatively affects both the mechanical and tribological properties of ALs. The mechanical properties decrease by a maximum of 41.04%, indicating that the number of spindles has the most significant effect on mechanical properties, while tribological properties deteriorates by a maximum of 22.07%.
3. Lowering the number of layers increases the breaking strain of ALs by 2.58%, and decreases the ultimate tensile force, elastic modulus and yield force by a maximum of 12.57%. However, the tribological properties are improved by a maximum of 53.60% with the decrease in the number of layers, indicating that the number of layers has the most significant effect on tribological properties.

Acknowledgements

This work was supported by the National Natural Science Foundation, China (Grant 52475205), Guangdong Basic and Applied Basic Research Foundation, China (Grants 2024A1515030208 and 2023A1515110565) and Shenzhen International Cooperation Research Project (Grant GJHZ20220913143005009).

Conflicts of Interest

The authors declare no conflicts of interest.

Data Availability Statement

The data that support the findings of this study are available from the corresponding author upon reasonable request.

References

1. M. Javed Awan, M. S. Mohd Rahim, N. Salim, M. Mohammed, B. Garcia-Zapirain, and K. Abdulkareem, "Efficient Detection of Knee Anterior Cruciate Ligament From Magnetic Resonance Imaging Using Deep Learning Approach," *Diagnostics* 11, no. 1 (2021): 105, https://doi.org/10.3390/diagnostics11010105.

2. N. Chen, W. Jin, H. Gao, et al., "Sequential Intervention of Anti-Inflammatory and Osteogenesis With Silk Fibroin Coated Polyethylene Terephthalate Artificial Ligaments for Anterior Cruciate Ligament Reconstruction," *Journal of Materials Chemistry B* 11, no. 34 (2023): 8281–8290, https://doi.org/10.1039/d3tb00911d.

3. J. W. Freeman, M. D. Woods, and C. T. Laurencin, "Tissue Engineering of the Anterior Cruciate Ligament Using a Braid–Twist Scaffold Design," *Journal of Biomechanics* 40, no. 9 (2007): 2029–2036, https://doi.org/10.1016/j.jbiomech.2006.09.025.

4. R. D'Ambrosi, A. Meena, E. S. Arora, M. Attri, L. Schäfer, and F. Migliorini, "Reconstruction of the Anterior Cruciate Ligament: A Historical View," *Annals of Translational Medicine* 11, no. 10 (2023): 364, https://doi.org/10.21037/atm-23-87.

5. M. Liden, L. Ejerhed, N. Sernert, G. Laxdal, and J. Kartus, "Patellar Tendon or Semitendinosus Tendon Autografts for Anterior Cruciate Ligament Reconstruction," *American Journal of Sports Medicine* 35, no. 5 (2007): 740–748, https://doi.org/10.1177/0363546506298275.

6. H. Numazaki, H. Tohyama, H. Nakano, S. Kikuchi, and K. Yasuda, "The Effect of Initial Graft Tension in Anterior Cruciate Ligament Reconstruction on the Mechanical Behaviors of the Femur-Graft-Tibia Complex During Cyclic Loading," *American Journal of Sports Medicine* 30, no. 6 (2002): 800–805, https://doi.org/10.1177/03635465020300060801.

7. E. Kondo, K. Yasuda, N. Kitamura, et al., "Effects of Initial Graft Tension on Clinical Outcome After Anatomic Double-Bundle Anterior Cruciate Ligament Reconstruction: Comparison of Two Graft Tension Protocols," *BMC Musculoskeletal Disorders* 17 (2016): 1–8, https://doi.org/10.1186/s12891-016-0909-y.

8. V. Viateau, M. Manassero, F. Anagnostou, S. Guérard, D. Mitton, and V. Migonney, "Biological and Biomechanical Evaluation of the Ligament Advanced Reinforcement System (LARS AC) in a Sheep Model of Anterior Cruciate Ligament Replacement: A 3-Month and 12-Month Study," *Arthroscopy: The Journal of Arthroscopic & Related Surgery* 29, no. 6 (2013): 1079–1088, https://doi.org/10.1016/j.arthro.2013.02.025.

9. C. M. Glezos, A. Waller, H. E. Bourke, L. J. Salmon, and L. A. Pinczewski, "Disabling Synovitis Associated With LARS Artificial Ligament Use in Anterior Cruciate Ligament Reconstruction: A Case Report," *American Journal of Sports Medicine* 40, no. 5 (2012): 1167–1171, https://doi.org/10.1177/0363546512438510.

10. D. Olvera, R. Schipani, B. N. Sathy, and D. J. Kelly, "Electrospinning of Highly Porous yet Mechanically Functional Microfibrillar Scaffolds at the Human Scale for Ligament and Tendon Tissue Engineering," *Biomedical Materials* 14, no. 3 (2019): 035016, https://doi.org/10.1088/1748-605x/ab0de1.

11. C. Vaquette, C. Kahn, C. Frochot, et al., "Aligned Poly (L-lactic-co-e-caprolactone) Electrospun Microfibers and Knitted Structure: A Novel Composite Scaffold for Ligament Tissue Engineering," *Journal of Biomedical Materials Research Part A* 94, no. 4 (2010): 1270–1282, https://doi.org/10.1002/jbm.a.32801.

12. K. R. Swank, A. W. Behn, and J. L. Dragoo, "The Effect of Donor Age on Structural and Mechanical Properties of Allograft Tendons," *American Journal of Sports Medicine* 43, no. 2 (2015): 453–459, https://doi.org/10.1177/0363546514557246.

13. I. Mabe and S. Hunter, "Quadriceps Tendon Allografts as an Alternative to Achilles Tendon Allografts: A Biomechanical Comparison," *Cell and Tissue Banking* 15, no. 4 (2014): 523–529, https://doi.org/10.1007/s10561-014-9421-5.

14. S. Lettry, F. Roccavilla, and B. B. Seedhom, "Abrasion of Artificial Ligaments: A Simulative Study," *Journal of Orthopaedic Science* 5 (2000): 481–488, https://doi.org/10.1007/s007760070027.

15. J. Song, D. Xiang, S. Wang, et al., "In Vitro Wear Study of PEEK and CFRPEEK Against UHMWPE for Artificial Cervical Disc Application," *Tribology International* 122 (2018): 218–227, https://doi.org/10.1016/j.triboint.2018.02.034.

16. C. Jiang, K. Wang, Y. Liu, C. Zhang, and B. Wang, "Application of Textile Technology in Tissue Engineering: A Review," *Acta Biomaterialia* 128 (2021): 60–76, https://doi.org/10.1016/j.actbio.2021.04.047.

17. M. F. Guidoin, Y. Marois, J. Bejui, N. Poddevin, M. W. King, and R. Guidoin, "Analysis of Retrieved Polymer Fiber Based Replacements for the ACL," *Biomaterials* 21, no. 23 (2000): 2461–2474, https://doi.org/10.1016/s0142-9612(00)00114-9.

18. M. Giordano, S. Schmid, M. Arjmandi, and M. Ramezani, "Wear Evaluation of Three-Dimensionally Woven Materials for Use in a Novel Cartilage Replacement," *Wear* 386 (2017): 179–187, https://doi.org/10.1016/j.wear.2017.06.012.

19. S. Li, S. Wang, J. Shao, et al., "Toward the Improvement of the Mechanical and Tribological Properties of Braided Ligament for ACL Reconstruction: A 'Carrot and Stick' Strategy," *Advanced Healthcare Materials* 13, no. 20 (2024): 2304133, https://doi.org/10.1002/adhm.202304133.

20. J. A. Cooper, H. H. Lu, F. K. Ko, J. W. Freeman, and C. T. Laurencin, "Fiber-Based Tissue-Engineered Scaffold for Ligament Replacement: Design Considerations and In Vitro Evaluation," *Biomaterials* 26, no. 13 (2005): 1523–1532, https://doi.org/10.1016/j.biomaterials.2004.05.014.

21. A. Pagán, S. D. Aznar-Cervantes, J. Pérez-Rigueiro, L. Meseguer-Olmo, and J. L. Cenis, "Potential Use of Silkworm Gut Fiber Braids as Scaffolds for Tendon and Ligament Tissue Engineering," *Journal of Biomedical Materials Research Part B: Applied Biomaterials* 107, no. 7 (2019): 2209–2215, https://doi.org/10.1002/jbm.b.34300.

22. N. Jiang and H. Hu, "Auxetic Yarn Made With Circular Braiding Technology," *Physica Status Solidi* 256, no. 1 (2019): 1800168, https://doi.org/10.1002/pssb.201800168.

23. R. C. Bray, P. T. Salo, I. K. Lo, P. Ackermann, J. B. Rattner, and D. A. Hart, "Normal Ligament Structure, Physiology and Function," *Sports Medicine and Arthroscopy Review* 13, no. 3 (2005): 127–135, https://doi.org/10.1097/01.jsa.0000173231.38405.ad.

24. M. C. Lu, Y. T. Huang, J. H. Lin, et al., "Evaluation of a Multi-Layer Microbraided Polylactic Acid Fiber-Reinforced Conduit for Peripheral Nerve Regeneration," *Journal of Materials Science: Materials in Medicine* 20, no. 5 (2009): 1175–1180, https://doi.org/10.1007/s10856-008-3646-4.

25. C. P. Laurent, D. Durville, D. Mainard, J. F. Ganghoffer, and R. Rahouadj, "A Multilayer Braided Scaffold for Anterior Cruciate Ligament: Mechanical Modeling at the Fiber Scale," *Journal of the Mechanical Behavior of Biomedical Materials* 12 (2012): 184–196, https://doi.org/10.1016/j.jmbbm.2012.03.005.